IEEE Access
Multidisciplinary ⋮ Rapid Review ⋮ Open Access Journal

Received 10 February 2024, accepted 26 February 2024, date of publication 29 February 2024, date of current version 8 March 2024.

Digital Object Identifier 10.1109/ACCESS.2024.3371518

RESEARCH ARTICLE

Group Teaching Optimization With Deep Learning-Driven Osteosarcoma Detection Using Histopathological Images

SHTWAI ALSUBAI[1], ASHIT KUMAR DUTTA[2], FAISAL ALGHAYADH[2], RAFIULLA GILKARAMENTHI[3], MOHAMAD KHAIRI ISHAK[4], FATEN KHALID KARIM[5], SAMEER ALSHETEWI[6], AND SAMIH M. MOSTAFA[7,8]

[1]Department of Computer Science, College of Computer Engineering and Sciences in Al-Kharj, Prince Sattam bin Abdulaziz University, Al-Kharj 11942, Saudi Arabia
[2]Department of Computer Science and Information Systems, College of Applied Sciences, AlMaarefa University, Diriyah, Riyadh 13713, Saudi Arabia
[3]Department of Emergency Medical Services, College of Applied Sciences, AlMaarefa University, Diriyah, Riyadh 13713, Saudi Arabia
[4]Department of Electrical and Computer Engineering, College of Engineering and Information Technology, Ajman University, Ajman, United Arab Emirates
[5]Department of Computer Sciences, College of Computer and Information Sciences, Princess Nourah bint Abdulrahman University, P.O. Box 84428, Riyadh 11671, Saudi Arabia
[6]Ministry of Defence, The Executive Affairs Excellence Services Directorate, General Information Technology Department, Riyadh 11671, Saudi Arabia
[7]Computer Science Department, Faculty of Computers and Information, South Valley University, Qena 83523, Egypt
[8]Faculty of Industry and Energy Technology, New Assiut Technological University (NATU), New Assiut City 71684, Egypt

Corresponding author: Samih M. Mostafa (samih_montser@sci.svu.edu.eg)

This work was supported by Princess Nourah bint Abdulrahman University Researchers Supporting Project number (PNURSP2024R300), Princess Nourah bint Abdulrahman University, Riyadh, Saudi Arabia.

ABSTRACT Osteosarcoma is the most normal kind of cancer that arises in bones, which appears on the surface to resemble earlier types of bone cells that assist in forging new bone tissues, but the tissue in osteosarcoma is weaker and softer than normal bone tissue. The usage of automated techniques for the detection of osteosarcoma has the potential to mitigate the obligations and burdens confronted by pathologists owing to its abundant quantity of cases. Artificial intelligence (AI) has an emerging progress in diagnostic pathology. In recent years, numerous studies using deep learning (DL) techniques to histopathological images (HI) have been published. While several studies claim higher accuracy, they might lack generalization and fall into the pitfall of overfitting owing to the wide range of HI. The study objective is to enhance the diagnosis and detection of osteosarcoma by employing computer-assisted detection (CAD) and diagnoses (CADx). Technique like convolutional neural networks (CNN) make better prognoses for patient conditions and considerably reduce the surgeon's workload. CNN needs to be trained on the massive quantity of data to accomplish a remarkable performance. Therefore, the study presents a novel Group Teaching Optimization Algorithm with Deep Learning-Driven Osteosarcoma Detection on Histopathological Images (GTOADL-ODHI) technique. The purpose of the GTOADL-ODHI technique is to examine the HIs for the detection and classification of osteosarcoma. To accomplish this, the GTOADL-ODHI algorithm applies the Gaussian filtering (GF) method for image pre-processed to become rid of the noise. Besides, the capsule network (CapsNet) model is utilized for the extractor of the feature vector. Furthermore, the hyperparameter selection of the CapsNet approach takes place using the GTOA. Finally, the self-attention bidirectional long short-term memory (SA-BiLSTM) model can be employed for osteosarcoma recognition and classification. The widespread experimental analysis of the GTOADL-ODHI method is tested on the benchmark datasets. The simulation validation reported the optimum solution of the GTOADL-ODHI algorithm related to existing systems concerning distinct aspects.

INDEX TERMS Bone cancer detection, CAD, histopathological image, deep learning, hyperparameter selection.

The associate editor coordinating the review of this manuscript and approving it for publication was Vishal Srivastava.

I. INTRODUCTION

Osteosarcoma is a malignant tumour that arises from bone and rapidly develops to form bone cancer [1]. It is the most

common type of orthopaedic disease. In general, osteosarcoma easily occurs at the upper end of the humerus, and tibia and, the low end of the femur, especially near the knee joint. Osteosarcoma tends to occur in teenagers and young people, and its symptoms include soreness, minor local bone pain, and fever at the tumour spot [2], [3]. Meanwhile, numerous cancers do not consume the usual image features, it is complex to define the mass nature by trusting only image analyses, and it is very difficult to define whether a patient is suffering from bone cancer or not. Osteosarcoma has numerous subtypes with dissimilar features of pathological [4]. Therefore, all specialists in osteosarcoma analysis consider the pathological analysis.

Digital pathology pictures are attained by scanning pathology images. The data dimensions of the image are huge, and one histopathological unit holds many numbers of cells [5]. The difficult pathological osteosarcoma features need very professional as well as experienced pathologists. The quantity of experienced pathologists is very limited and every professional processes numerous slices daily [6]. It is very significant to improve a proper decision diagnosis method for histopathological images (HIs) to help pathologists analyze osteosarcoma and improve the issues that occur in hospitals [7]. With the improvement and spread of artificial intelligence (AI) techniques [8], neural networks play a significant part in medical field analysis with their great feature extractor capability like MRI segmentation of osteosarcoma, auxiliary staging of lung cancer, and others [9]. Machine learning (ML) techniques are the present advanced techniques for image classification [10]. As well as Deep learning (DL) architectures like Vision Transformers (ViTs) and Convolutional Neural Networks (CNNs) have attained exciting outcomes when compared to human performance in numerous tasks. CNNs are normally employed for automatic data removal from image data [11]. Numerous CNN frameworks are projected that manage such issues in unique methods and are employed affording to the necessity [12].

This study presents an innovative Group Teaching Optimizer Algorithm with DL-driven osteosarcoma Detection on Histopathological Images (GTOADL-ODHI) technique. The purpose of the GTOADL-ODHI technique is to examine the HIs for the recognition and classification of osteosarcoma. Initially, the GTOADL-ODHI technique applies the Gaussian filtering (GF) method for noise removal process. Besides, the capsule network (CapsNet) model is utilized for the extractor of the feature vector. Furthermore, the hyperparameter selection of the CapsNet approach takes place using the GTOA. Finally, the self-attention bidirectional long short-term memory (SA-BiLSTM) model can be employed for osteosarcoma recognition and classification. The simulation study of the GTOADL-ODHI technique is the tested on the benchmark datasets. The key contributions are summarized as follows.

- Improves a holistic technique for osteosarcoma recognition by merging feature extraction utilizing CapsNet, enhanced hyperparameter range with GTOA, and identification utilizing the SA-BiLSTM method. This complete pipeline develops the general accuracy and reliability of osteosarcoma recognition on histopathological imageries.
- Apply CapsNet as the feature vector extraction. CapsNet is recognized for its capability to take hierarchical relations and spatial hierarchies in difficult structures, creating it appropriate for removing features from histopathological images.
- Use GTOA as an advanced optimizer model. GTOA is exactly intended to improve the hyperparameter selection procedure for the CapsNet technique that is employed in osteosarcoma recognition. The usage of GTOA for CapsNet hyperparameter tuning procedure validates the innovation of the work.
- Present the SA-BiLSTM method for osteosarcoma detection and identification. SA-BiLSTM is a new structure that combines the profits of self-attention devices and BiLSTM for enhanced sequential data study, paying for more precise classification outcomes.

II. LITERATURE WORKS

In [13], a structure that removes features depending on CNN is presented. Foremost, data augmentation is utilized in order to spread the dataset size. Then, the technique chiefly measured six pre-trained transfer learning (TL) techniques and adapted the techniques to remove features. Next, the technique inspected feature selection (FS) such as Recursive Feature Elimination, Principal Component Analysis, and Genetic Algorithm, and Baruto found PCA picks an optimum set of features. Lastly, the research sends the nominated features into a finetuned MLP termed Grid Search MLP (GsMLP) and uses federated learning (FL) models. Badashah et al. [14] proposed an effectual recognition technique utilizing the developed Fractional Harris Hawks Optimizer-based GAN (FHHO-GAN) technique. The classification of viable tumor, non-tumour, and necrotic cancer has been implemented by GAN utilizing the HI slides. GAN has been employed to execute the osteosarcoma diagnoses. Bansal et al. [15] projected an automatic diagnosis method namely Integrated Features-FS Model for Classification (IF-FSM-C) technique.

This technique merged the features extraction employing traditional handcrafted (HC) feature extractor models and DL techniques such as EfficientNet-B0 and Xception. Then, FS is implemented. Here, the Arithmetic Optimizer Algorithm (AOA) also recognized as BAOA-V and BAOA-S was developed to execute FS, and is assumed to be a classifier that categorizes the WSIs.

Prabakaran and Mary Praveena [16] developed a new hyperparameter-tuned DL technique. The Harmonic Mean-based Otsu Thresholding (HMOTH) and Median Filtering (MEF) are utilized for pre-processing and segment process, which is later removed by employing the Self Attention Mechanism-based MobileNet (SAMMNet) method. An adaptive Inertia Weight and Vander Corput sequence comprised Reptile Search Optimizer Algorithm

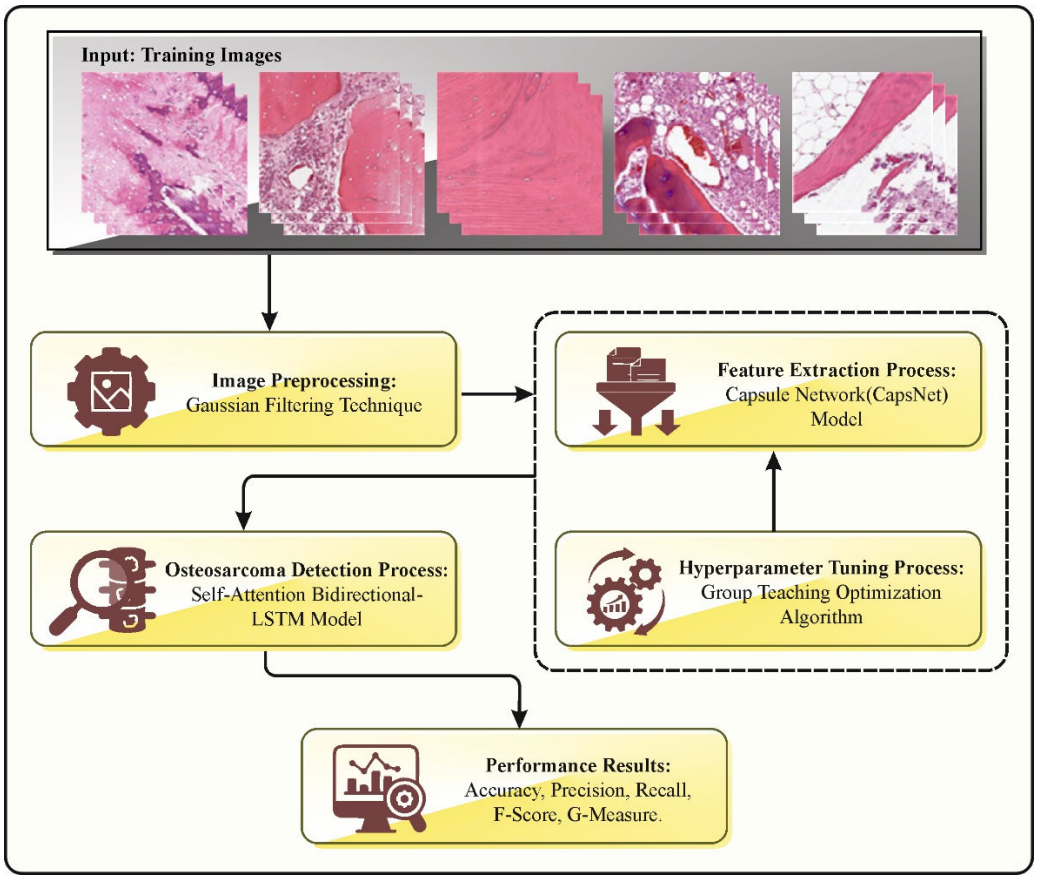

FIGURE 1. Overall flow of GTOADL-ODHI method.

(VARSOA) can be utilized to pick the further related features. Lastly, a Hyperparameter-Tuned Deep ENN (HTDENN) has been used. Ahmed et al. [17] offer a compact CNN architecture. This technique presents an oversampling method. During this procedure, a hierarchical CNN technique has been designed, but the previous method is non-regularized owing to its dense structure and the latter one has been normalized, specially intended for minor HIs. Furthermore, the normalized technique is combined with CNN's basic structure to decrease over-fitting. Shen et al. [18] examine an osteosarcoma-assisted segmentation technique depending on the guided aggregated bilateral network (OSGABN) model, which is a great accuracy method with a lightweight semantic branch that captures rich semantic framework and a detailed branch that captures lowest-level data.

Asito et al. [19] present to divide the images in windows and separately categorize them by employing a CNN. Approaches for pre-processed like window exclusion and labelling have been projected. Dual CNNs have been equated in the developed method. The primary one is trained from scratch, but the 2nd one is a pre-trained CNN (VGG16). The CNNs are equated to 4 ML techniques namely DT, MLP, and RF with FS. In [20], a hybrid structure is presented. After pre-processing, five pre-trained CNN approaches were proficient with manifold parameter settings to remove perceptive features through TL. For FS, a decision tree-based RFE has been intended. At this point, a DT has been employed as an estimation to pick the dissimilar features. Lastly, an improved MLP classifier has been used to categorize into two and multi-class kinds of osteosarcoma under the 5-fold CV for estimation.

Priyadharshini et al. [21] presents an innovative hybrid Extreme Learning Machine (ELM) and Teaching–Learning-Based Optimizer (TLBO) approach as a versatile method for identifying melanoma. ELM is a single-hidden layer feed-forward neural network that can be proficient rapidly and precisely, whereas TLBO is an optimizer algorithm employed to modify the network's parameters for enhanced performance. Eysa [22] projects an intelligent technique for analyzing colorectal cancer. The developed model employs the group teaching optimizer model for feature selection to pick the vital image features for plant disease. This feature employs to absorb the multi-layer artificial neural network (ANN) to categorize images into dual classes namely normal and malignant. Lal et al. [23] project a NucleiSegNet - a robust DL network structure for the nuclei segmentation of H&E-stained liver cancer histopathology images. Our developed architecture contains 3 blocks such as a robust

bottleneck block, an attention decoder block and a residual block. Ahmad et al. [24] presents a new spatial-channel attention-based altered UNet architecture with ResNet blocks in encoder layers. The UNet baseline preserves rough and fine features, thus verifying the solution to the tissue variability.

III. THE PROPOSED MODEL

In this study, a novel GTOADL-ODHI method is established. The purpose of the GTOADL-ODHI technique is to examine the HIs for the recognition and classification of osteosarcoma. To accomplish this, the GTOADL-ODHI technique contains GF-based preprocessing, CapsNet-based feature extractor, GTOA-based hyperparameter tuning, and SA-BiLSTM-based classification. Fig. 1 shows the workflow of the GTOADL-ODHI technique.

A. GF BASED PREPROCESSING

At the primary level, the GTOADL-ODHI technique applies the GF technique for image preprocessing to remove the noise. GF is an extensively deployed image preprocessing approach that comprises convolving an image with Gaussian function to blur or smooth the image, decreasing noise and increasing essential features [25]. The filter allocates superior weights to pixels near the center; slowly reducing as distance upsurges, reflecting the bell-shaped Gaussian distribution. These performances in a weight-averaging outcome that efficiently reduces higher-frequency noise while maintaining the entire design and edges of images. GF determines applications in several fields comprising noise reduction, image smoothing, and feature extractor, in performance a vital play in enhancing image quality and enabling subsequent CV tasks.

B. FEATURE EXTRACTOR

For the feature extractor process, the CapsNet model can be used for the extraction of the feature vectors. CapsNet has been developed the capsule to mitigate the drawbacks of CNNs [26]. A pooling layer of CNN loses several key features while resizing and extracting the features. Furthermore, a CNN could not learn the relation among the features extracted due to the lack of function able to obtain the essential data. Like the pooling layer in CNN, CapsNet makes use of the squash function. This function doesn't lose any data because it is a non-linear function that accepts input in the form of a vector and resizes the data in the unit vector as mathematically given below:

$$\hat{u}_{j|i} = W_{ij^u i} \tag{1}$$

In Eq. (1), the prediction vector produced by i^{th} capsules that are passed to *the* j^{th} capsule is represented as $\hat{u}$ and evaluated by multiplying *the* W_{ij} weight matrix with the *ui* output of *the* i^{th} prior capsule layer.

$$s_j = \sum_i c_{ij}\hat{u}_{j|i} \tag{2}$$

In CapsNet, a typical CNN neuron is replaced by the capsule, and the input and output units are transformed into vectors. The capsule vector length signifies the probability that the entity exists in an input. Similar to the activation function of CNN, the "squashing" function makes sure that the vector length is between zero and one as follows:

$$v_j = \frac{||s||^2}{1 + ||s||^2}\frac{s_j}{||s_j||} \tag{3}$$

In Eq. (3), v_j and s_j are the output and input vectors of j^{th} capsules.

$$c_{ij} = \frac{\exp(b_{ij})}{\sum_j \exp(b_{ij})} \tag{4}$$

In Eq. (2), the coupling coefficient c_{ij} is represented as the dynamic routing mechanism. The aim is to enable the input capsule to select its track for communication to the following capsule layers. c_{ij} refers to the softmax function over b_{ij}, representing the prior log probability between *the* i^{th} and j^{th} capsules. CapsNet exploits the b_{ij} parameter to define the relations between the i^{th} and j^{th} capsules in the prior layers. During the initial iteration, b_{ij} is initialized to 0 and the value of coupling co-efficient c_{ij} is similar to each capsule within the layer. v_j and $\hat{u}_{j|i}$ values are upgraded by employing Eqs. (3) & (1), correspondingly. The b_{ij} a parameter was upgraded by the $\hat{u}$ and v_j dot products in succeeding iteration:

$$b_{ij} = b_{ij} + \hat{u}_{j|i}v_j \tag{5}$$

Once the dot products of $\hat{u}_{j|i}$ and v_j are negative, then the relationship between i^{th} and j^{th} capsules are weakened. Once the dot products of $\hat{u}_{j|i}$ and v_j produce a positive outcome, then b_{ij} has a bigger value. A bigger value for b_{ij} will lead to the greatest value for c_{ij}, resulting in the greatest values for s_j and v_j, strengthening the relationship among i^{th} and j^{th} capsules.

C. HYPERPARAMETER TUNING USING GTOA

At this stage, the hyperparameter selection of the CapsNet technique takes place using GTOA. The GTOA is an effective and novel metaheuristic optimization technique whose main idea originates from the group teaching model [27]. The GTOA consists of the teacher stage, student stage, teacher allocation stage, and ability grouping stage. The Initialization and four stages of GTOA are discussed below.

1) INITIALIZATION

The population can be initialized by the N individuals, representing the N students. The initial individual is X_i^t=($x_{i,1}^t, \ldots, x_{i,j}^t, \cdots, {}^t_{xi,D}$), where D symbolizes the number of optimizer parameters; the count of generations with primary value t= 0 is denoted by t. The mathematical formula can be given as follows.

$$X_i^t = X^L + e_i(X^U - X^L)i = 1, \ldots, N \tag{6}$$

Here, the i^{th} student at t^{th} generation is represented as X_i^t; the lower and upper boundaries of the population are X^L and X^U; the uniform distribution random vector is $e_j \in [0, 1]^D$.

2) TEACHER ALLOCATION PHASE

'Teacher' is designated as the student with the best calculation score after the initialization stage is accomplished. This determines the fitness of each student.

$$T^t = \begin{cases} X^t_{first} & if\ f(X^t_{first}) \leq f\left(\dfrac{X^t_{first} + X^t_{second} + X^t_{third}}{3}\right) \\ \dfrac{X^t_{first} + X^t_{second} + X^t_{third}}{3} & otherwise \end{cases} \tag{7}$$

where the teacher chosen from the population is represented as T^t; the 3 students with the 1st, 2nd, and 3rd scores in the population are X^t_{first}, X^t_{second}, and X^t_{third}, correspondingly.

3) ABILITY GROUPING PHASE

The group with low scores and the outstanding group with high scores are the two groups of students according to their scores. In the minimization problem, the common group has a higher objective value than the outstanding group.

4) TEACHER PHASE

With the knowledge base and higher test scores, the teacher attempts to enhance the scoring capability of each student from the classroom, thus increasing the test score. The teacher teaches common and outstanding students in different ways. Using Eq. (8), the student in the outstanding group updates the position, and using Eq. (9), the student in the common group updates the position.

$$X^{t+1}_{teacher,i} = X^t_i + a \times \left(T^t - F \times \left(b \times M^t + c \times X^t_i\right)\right) \tag{8}$$

$$X^{t+1}_{teacher,i} = X^t_i + 2 \times d \times \left(T^t - X^t_i\right) \tag{9}$$

where the i^{th} students who have passed the teacher stage at t^{th} generation are represented as $X^{t+1}_{teacher,i}$; X^t_i represents the i^{th} student at t^{th} generation; shows the average location of the student in the class is denoted by $M^t = \frac{1}{N}\sum_{i=1}^{N} X^t_i, M^t$; F signifies the teaching factor arbitrarily selected from one or two; a, b, c, and d are the arbitrary integers from zero and one and $b + c = 1$. After the teacher phase, the student updates the position using the following equation:

$$X^{t+1}_{teacher,i} = \begin{cases} X^{t+1}_{teacher,i} & if\ \left(^{t+1}_{teacher,i}\right) \leq f\left(X^t_i\right) \\ X^t_i & otherwise \end{cases} \tag{10}$$

5) STUDENT PHASE

In this phase, student communicates with one another to further enhance the overall scoring capability. Note that common and outstanding groups only interact within their corresponding groups using the subsequent expression:

$$X^{t+1}_{student,i}$$

$$= \begin{cases} X^{t+1}_{teacher,i} + e \times \left(X^{t+1}_{teacher,i} - X^{t+1}_{teacher,j}\right) \\ +g \times \left(X^{t+1}_{teacher,i} - X^t_i\right)\ iff\ \left(X^{t+1}_{teacher,i}\right) \leq f\left(X^{t+1}_{teacher,j}\right) \\ X^{t+1}_{teacher,i} - e \times \left(X^{t+1}_{teacher,i} - X^{t+1}_{teacher,j}\right) \\ +g \times \left(X^{t+1}_{teacher,i} - X^t_i\right)\ otherwise \end{cases} \tag{11}$$

In Eq. (11), e and g are the arbitrary real numbers in zero and one. The i^{th} and j^{th} student who has passed the teacher stage at t^{th} generation is represented as $X^{t+1}_{teacher,i}$ and $X^{t+1}_{teacher,j}(j \neq i)$. After, the students update the position based on the following equation:

$$X^{t+1}_i = \begin{cases} X^{t+1}_{teacher,i} & iff(X^{t+1}_{teacher,i}) \leq f(X^{t+1}_{student,i}) \\ X^{t+1}_{student,i} & otherwise \end{cases} \tag{12}$$

The GTOA system produces a fitness function (FF) to make great classifier outcomes. It defines a positive integer to imply the best solution of candidate results. Now, the reduction of the classifier error rate is assumed as FF.

$$\begin{aligned} fitness\,(x_i) &= Classifier\ Error\ Rate\,(x_i) \\ &= \frac{No.of\ misclassified\ instances}{Total\ no.of\ instances} * 100 \end{aligned} \tag{13}$$

D. SA-BILSTM-BASED CLASSIFICATION

Eventually, the SA-BiLSTM model can be employed for osteosarcoma detection and classification. Recurrent Neural Network (RNN) is most commonly used to predict time sequence datasets due to the capability to learn relationships between information from prior and present moments [28]. However, RNNs face challenges in capturing the relationship as the prediction time horizon increases, resulting in a subsequent decline in forecast accuracy and the problem of gradient disappearance.

Hochreiter and Schmidhuber in 1997, established the LSTM model to resolve these problems. LSTM successfully lessens the vanishing gradient problems by integrating the cellular state for retaining long-term memory along with the latent state of RNN. The LSTM model includes three gates: forget, input, and output gates. In addition, the computation equation governing the LSTM block is used for effective computation.

$$l_t = \sigma\left(W_i \cdot [h_{t-1}, X_t] + b_i\right) \tag{14}$$

$$F_t = \sigma(W_f \cdot \left[[h_{t-1}, X_t] + b_f\right) \tag{15}$$

$$\mathrm{O}_t = \sigma(W_o \cdot [[h_{t-1}, X_t] + b_o) \tag{16}$$

$$\tilde{C}_{\mathrm{t}} = tanh(W_c \cdot [[h_{t-1}, X_t] + b_c) \tag{17}$$

$$C_t = F_t \times C_{t-1} + l_t \times \tilde{C}_t \tag{18}$$

$$h_t = \mathrm{O}_t \cdot tanh\,(\mathrm{C_t}) \tag{19}$$

From the equations, σ indicates the sigmoid function. I_t indicates the input gate, F_t shows the forget gate, 0τ represents the output gate, C_τ shows the cell layer at t time, W_i, W_f, W_o, W_u stands for the corresponding weight

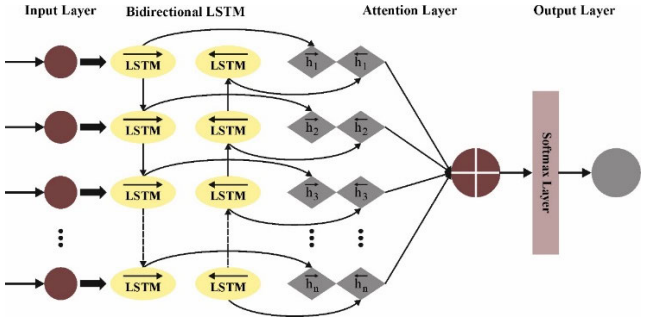

FIGURE 2. Framework of BiLSTM technique.

matrix, b_i, b_f, b_o, b_u symbolize the corresponding bias terms. It collects only the knowledge regarding the previous input dataset while LSTM addresses the problem of long-term dependency. The existing state might be tied to prior or present data for the long-time sequence problems. At the same time, BiLSTM includes two LSTM models functioning in opposing directions that extract the features of the input dataset. The data transmission in the BiLSTM is similar to the LSTM. The last output can be covered by the LSTM output in both directions. The data extracted by the CNN feature is fed into the Bi-LSTM approach, and the dual-layer prediction models forecast the result. SA-BiLSTM model deployed self-attention to improve its ability to correctly capture the connection between pre-and-post-water-temperature data. Fig. 2 illustrates the infrastructure of BiLSTM. Employing a self-attention model, this method develops accomplished at identifying long-term dependency from the data series before and after a certain point. Accordingly, this method obtains the capability to focus on essential data points that mostly affect the predictive method, allocating them superior weights but downplaying the significance of lesser vital data by allocating them lesser weight. It is formulated as:

$$Q = X_t \cdot W^Q \tag{20}$$

$$K = X_t \cdot W^K \tag{21}$$

$$V = X_t \cdot W^V \tag{22}$$

In the training stage, the parameters W^Q, W^K, *and* W^V are learned, and the softmax function can be executed to obtain the normalization attention-weighted matrix α. The α matrix has been normalized column-by-column utilizing a certain normalized function can be computed as:

$$\alpha = sofrma\chi\left(QK^T\right) \tag{23}$$

$$Atten = Attention\,(Q, K, V) = \alpha V \tag{24}$$

Eventually, it can utilize the attention weights α to make a weighted sum and H_i^{a} on every resultant vector of the Bi-LSTM layer with the next formula:

$$H_i^{\mathrm{a}} = \sum_{j=1}^{m} \alpha_{ij} V_j \tag{25}$$

TABLE 1. Details on database.

Class Labels	No. of Images
Non-Tumor	536
Non-Viable Tumor	263
Viable-Tumor	345
Total Images	1144

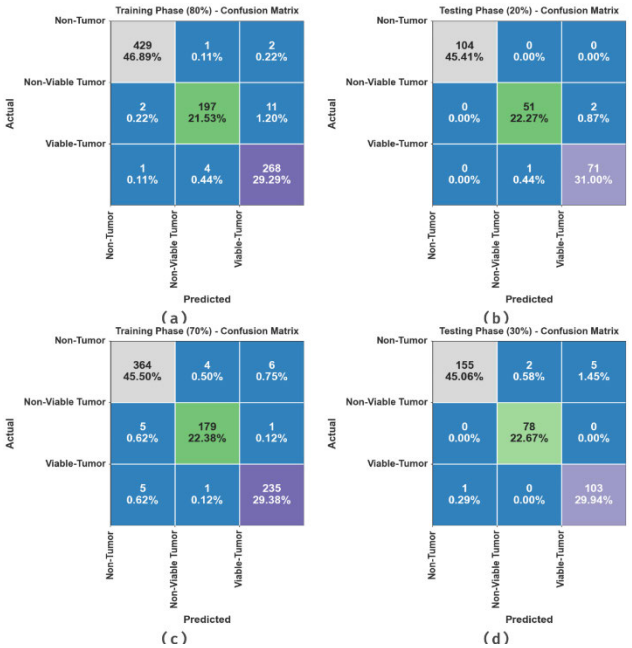

FIGURE 3. Confusion matrices of (a-b) 80:20 of TRPH/TSPH and (c-d) 70:30 of TRPH/TSPH.

TABLE 2. Classifier result of GTOADL-ODHI technique under 80:20 of TRPH/TSPH.

Classes	$Accu_y$	$Prec_n$	$Reca_l$	F_{Score}	$G_{Measure}$
TRPH (80%)					
Non-Tumor	99.34	99.31	99.31	99.31	99.31
Non-Viable Tumor	98.03	97.52	93.81	95.63	95.65
Viable-Tumor	98.03	95.37	98.17	96.75	96.76
Average	98.47	97.40	97.09	97.23	97.24
TSPH (20%)					
Non-Tumor	100.00	100.00	100.00	100.00	100.00
Non-Viable Tumor	98.69	98.08	96.23	97.14	97.15
Viable-Tumor	98.69	97.26	98.61	97.93	97.93
Average	99.13	98.45	98.28	98.36	98.36

$$\sum_{j=1}^{m} \alpha_{ij} = 1, i \in \{1, 2, \ldots, m\} \tag{26}$$

In which, α_{ij} is an attention vector at the i^{th} location, signifying the attention received at *the*j^{th} position.

IV. RESULT ANALYSIS

In this section, the stimulation analysis of the GTOADL-ODHI technique is tested utilizing the dataset including 1144 samples with three class labels as signified in Table 1.

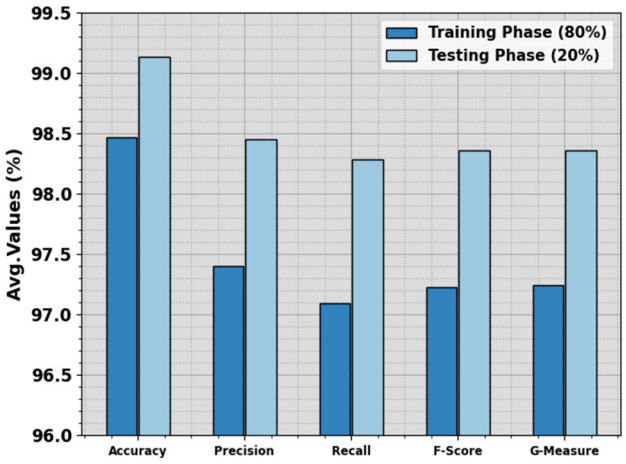

FIGURE 4. Average of GTOADL-ODHI technique on 80:20 of TRPH/TSPH.

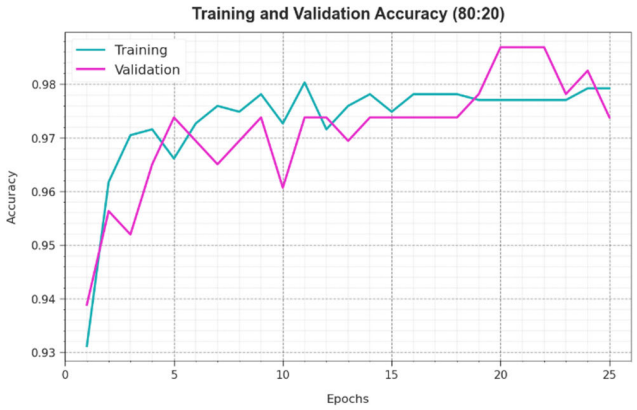

FIGURE 5. $Accu_y$ curve of GTOADL-ODHI technique under 80:20 of TRPH/TSPH.

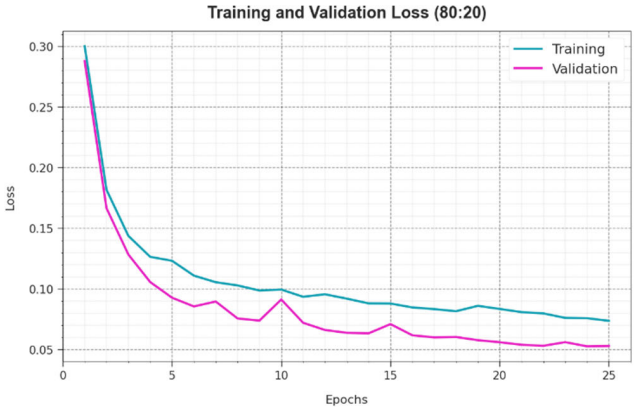

FIGURE 6. Loss curve of GTOADL-ODHI method under 80:20 of TRPH/TSPH.

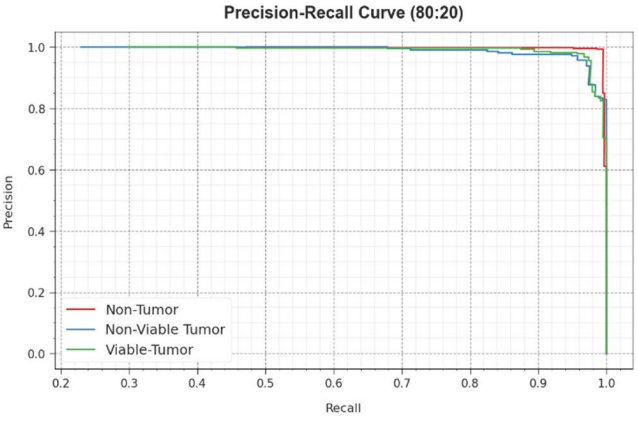

FIGURE 7. PR curve of GTOADL-ODHI method under 80:20 of TRPH/TSPH.

This study utilized the Osteosarcoma Tumor Assessment dataset, available at https://wiki.cancerimagingarchive.net/plugins/ servlet/mobile?contentId=52756935#content/view/52756935.

Fig. 3 validates the confusion matrices offered by the GTOADL-ODHI technique at 80:20 and 70:30 of TRPH/TSPH. The outcomes specify the effective recognition and detection of all three class labels properly.

In Table 2 and Fig. 4, the overall classification performance of the GTOADL-ODHI algorithm can be portrayed. The outcomes infer that the GTOADL-ODHI method obtains effective identification of classes.

With 80% of TRPH, the GTOADL-ODHI technique offers an average $accu_y$ of 98.47%, $prec_n$ of 97.40%, $reca_l$ of 97.09%, F_{score} of 97.23%, and $G_{measure}$ of 97.24%. Additionally, with 20% of TSPH, the GTOADL-ODHI model provides an average $accu_y$ of 99.13%, $prec_n$ of 98.45%, $reca_l$ of 98.28%, F_{score} of 98.36%, and $G_{measure}$ of 98.36%.

The $accu_y$ curves for training (TR) and validation (VL) displayed in Fig. 5 for the GTOADL-ODHI method at 80:20 of TRPH/TSPH provide valuable insights into its performance under numerous epochs. Particularly, there is a steady development in both TR and TS $accu_y$ to growing epochs, designating the model's ability to learn and identify patterns from both TR and TS data. The upward trend in TS $accu_y$ underlines the model's flexibility to the TR dataset and its capability to create precise forecasts on unseen data, prominence robust generalized abilities.

Fig. 6 offers a complete summary of the TR and TS loss values for the GTOADL-ODHI method under 80:20 of TRPH/TSPH through numerous epochs. The TR loss steadily decreases as the model increases its weights to reduce classification faults on both datasets. The loss curves exemplify the model's position with the TR data, highlighting its ability to capture patterns in both datasets. Noteworthy is the continuous alteration of parameters in the GTOADL-ODHI approach, intended to diminish differences between forecasts and actual TR labels.

About the PR curve offered in Fig. 7, the outcomes approves that the GTOADL-ODHI technique at 80:20 of TRPH/TSPH gradually reaches improved PR values across each classes. These outcomes highpoint the model's actual capability for discerning between different classes, highlighting its efficacy in precisely recognizing classes.

Besides, in Fig. 8, ROC curves created by the GTOADL-ODHI technique under 80:20 of TRPH/TSPH, represent its ability in distinguishing amid the classes shown.

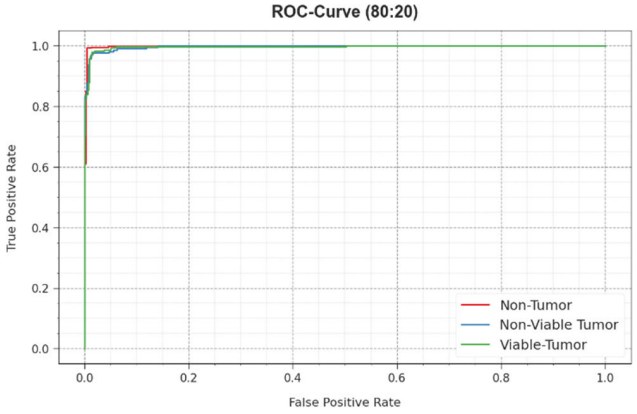

FIGURE 8. ROC curve of GTOADL-ODHI technique under 80:20 of TRPH/TSPH.

TABLE 3. Classifier result of GTOADL-ODHI technique on 70:30 of TRPH/TSPH.

Classes	$Accu_y$	$Prec_n$	$Reca_l$	F_{Score}	$G_{Measure}$
TRPH (70%)					
Non-Tumor	97.50	97.33	97.33	97.33	97.33
Non-Viable Tumor	98.62	97.28	96.76	97.02	97.02
Viable-Tumor	98.38	97.11	97.51	97.31	97.31
Average	98.17	97.24	97.20	97.22	97.22
TSPH (30%)					
Non-Tumor	97.67	99.36	95.68	97.48	97.50
Non-Viable Tumor	99.42	97.50	100.00	98.73	98.74
Viable-Tumor	98.26	95.37	99.04	97.17	97.19
Average	98.45	97.41	98.24	97.80	97.81

These curves deliver valuable insight into how the trade-off amongst TPR and FPR differs across dissimilar classification epochs and thresholds. The result underlines the model's accurate classification performance at several class labels, underscoring its efficiency in addressing various classification tasks.

In Table 3 and Fig. 9, the complete classification consequences of the GTOADL-ODHI approach can be represented. The results infer that the GTOADL-ODHI model attains effective identification of classes. With 70% of TRPH, the GTOADL-ODHI approach provides an average $accu_y$ of 98.17%, $prec_n$ of 97.24%, $reca_l$ of 97.20%, F_{score} of 97.22%, and $G_{measure}$ of 97.22%. Additionally, with 30% of TSPH, the GTOADL-ODHI model offers an average $accu_y$ of 98.45%, $prec_n$ of 97.41%, $reca_l$ of 98.24%, F_{score} of 97.80%, and $G_{measure}$ of 97.81%.

The $accu_y$ curves for TR and VL presented in Fig. 10 for the GTOADL-ODHI method under 70:30 of TRPH/TSPH offer valuable visions into its performance at numerous epochs., there is a reliable development in both TR and TS $accu_y$ to growing epochs, representing the model's ability to learn and identify designs from both TR and TS data. The upward trend in TS $accu_y$ highlights the model's flexibility

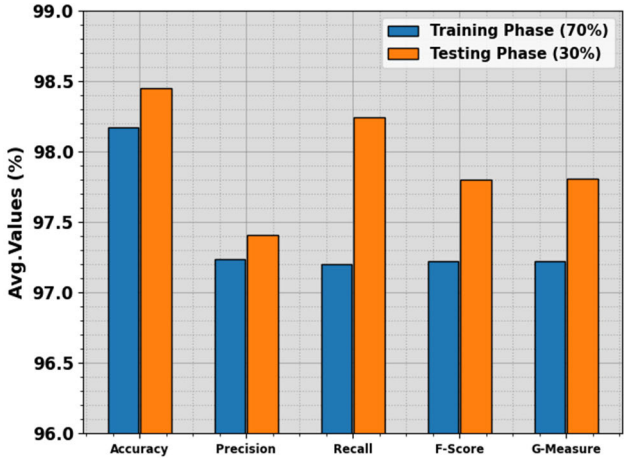

FIGURE 9. Average of GTOADL-ODHI technique under 70:30 of TRPH/TSPH.

FIGURE 10. $Accu_y$ curve of GTOADL-ODHI technique under 70:30 of TRPH/TSPH.

FIGURE 11. Loss curve of GTOADL-ODHI technique under 70:30 of TRPH/TSPH.

to the TR dataset and its capability to create precise forecasts on hidden data, emphasizing robust generalized capabilities.

Fig. 11 delivers a complete outline of the TR and TS loss values for the GTOADL-ODHI method on 70:30 of TRPH/TSPH across numerous epochs. The TR loss steadily

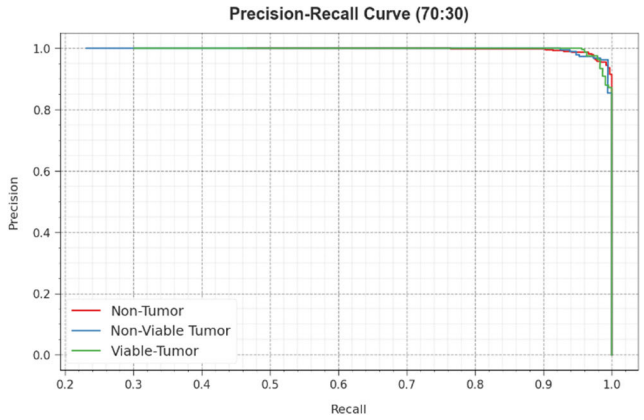

FIGURE 12. PR curve of GTOADL-ODHI technique under 70:30 of TRPH/TSPH.

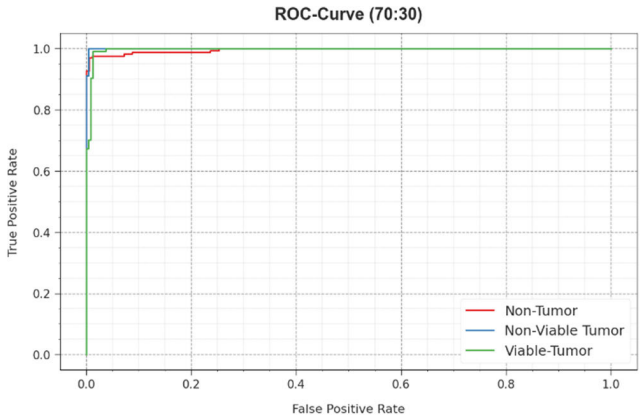

FIGURE 13. ROC curve of GTOADL-ODHI technique under 70:30 of TRPH/TSPH.

decreases as the technique increases its weights to lessen classification faults on both datasets. The loss curves exemplify the model's arrangement with TR data, highlighting its ability to capture patterns in both datasets. Noteworthy is the continuous modification of parameters in the GTOADL-ODHI model, intended to diminish differences among forecasts and real TR labels.

Regarding the PR curve offered in Fig. 12, the findings uphold that the GTOADL-ODHI technique below 70:30 of TRPH/TSPH reliably gets amended PR values across each class. These outcomes highlight the model's real ability to distinguish amid different classes, emphasizing its worth in accurately recognizing class labels.

Besides, in Fig. 13, ROC curves formed by the GTOADL-ODHI technique at 70:30 of TRPH/TSPH, representing its ability in distinguishing amongst classes. These curves deliver valuable insight into how the trade-off between TPR and FPR differs across dissimilar classification epochs and thresholds. These outcomes underline the model's accurate classification performance below many class labels, highlighting its efficacy in addressing different classification tasks.

In Table 4 and Fig. 14, the comparison study of the GTOADL-ODHI tactic with existing techniques was carried

TABLE 4. Comparative outcome of GTOADL-ODHI method with other existing algorithms [17].

Methods	$Accu_y$	$Prec_n$	$Reca_l$	F_{Score}
GTOADL-ODHI	99.13	98.45	98.28	98.36
Non-regularized CNN	98.00	92.92	94.31	96.91
Regularized CNN	84.00	80.50	86.36	85.88
AlexNet Model	94.30	95.16	94.35	97.71
DBN Model	96.71	96.43	94.41	96.57
XG-Boost Model	97.08	90.47	96.01	97.05
Random Forest	90.03	90.39	91.19	93.84
Naïve Bayes	96.36	93.20	90.54	92.48

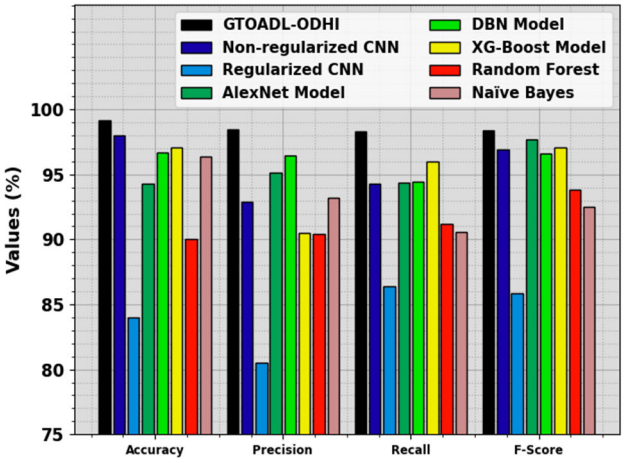

FIGURE 14. Comparative outcome of GTOADL-ODHI technique with other existing methods.

out [17]. The outcomes imply that the regularized CNN method reaches poor performance whereas the RF model obtains slightly improved performance. At the same time, AlexNet, DBN, XGBoost, and NB models accomplish closer results. Although the non-regularized CNN model reaches reasonable performance, the GTOADL-ODHI technique gains maximum performance with maximum $accu_y$ of 99.13%, $prec_n$ of 98.45%, $reca_l$ of 98.28%, and F_{score} of 98.36%.

Therefore, the GTOADL-ODHI method can be applied for automated osteosarcoma detection and classification processes.

V. CONCLUSION

In this study, a new GTOADL-ODHI algorithm is established. The purpose of the GTOADL-ODHI technique is to examine the HIs for the detection and classification of osteosarcoma. To accomplish this, the GTOADL-ODHI technique contains GF-based preprocessing, CapsNet-based feature extractor, GTOA-based hyperparameter tuning, and SA-BiLSTM-based classification process. At the primary level, the GTOADL-ODHI technique applies the GF technique for image pre-processing to get rid of the sound. Besides, the CapsNet model can be utilized for the extraction of the feature vectors. Additionally, the hyperparameter

selection of the CapsNet approach takes place using the GTOA. Finally, the SA-BiLSTM model can be employed for osteosarcoma recognition and classification. The widespread experimental analysis of the GTOADL-ODHI algorithm is tested on the benchmark datasets. The simulation validation reported a better performance of the GTOADL-ODHI approach compared to other methods with respect to various aspects.

ACKNOWLEDGMENT

Princess Nourah bint Abdulrahman University Researchers Supporting Project number (PNURSP2024R300), Princess Nourah bint Abdulrahman University, Riyadh, Saudi Arabia.

REFERENCES

[1] Z. Wang, J. Wu, C. Li, B. Wang, Q. Wu, L. Li, H. Wang, C. Tu, and J. Yin, "Diagnosis of osteosarcoma based on multimodal microscopic imaging and deep learning," *J. Innov. Opt. Health Sci.*, pp. 1–10, Feb. 2024, doi: 10.1142/S1793545823430010.

[2] F. Liu, J. Zhu, B. Lv, L. Yang, W. Sun, Z. Dai, F. Gou, and J. Wu, "Auxiliary segmentation method of osteosarcoma MRI image based on transformer and U-Net," *Comput. Intell. Neurosci.*, vol. 2022, pp. 1–16, Nov. 2022.

[3] Y. Hu, J. Tang, S. Zhao, and Y. Li, "Diffusion-weighted imaging-magnetic resonance imaging information under class-structured deep convolutional neural network algorithm in the prognostic chemotherapy of osteosarcoma," *Sci. Program.*, vol. 2021, pp. 1–12, Aug. 2021.

[4] Z. He, J. Liu, F. Gou, and J. Wu, "An innovative solution based on TSCA-ViT for osteosarcoma diagnosis in resource-limited settings," *Biomedicines*, vol. 11, no. 10, p. 2740, Oct. 2023.

[5] T. Asmaria, D. A. Mayasari, M. A. Heryanto, M. Kurniatie, R. Wati, and S. Aurellia, "Osteosarcoma classification using convolutional neural network," in *Proc. Int. Conf. Comput., Control, Informat. Appl.*, Oct. 2021, pp. 26–30.

[6] J. Wu, S. Yang, F. Gou, Z. Zhou, P. Xie, N. Xu, and Z. Dai, "Intelligent segmentation medical assistance system for MRI images of osteosarcoma in developing countries," *Comput. Math. Methods Med.*, vol. 2022, pp. 1–17, Jan. 2022.

[7] G. Xia, T. Ran, H. Wu, M. Wang, and J. Pan, "The development of mask R-CNN to detect osteosarcoma and oste-ochondroma in X-ray radiographs," *Comput. Methods Biomechanics Biomed. Engineering: Imag. Visualizat.*, vol. 11, no. 5, pp. 1869–1875, Sep. 2023.

[8] B. C. Mohan, "Osteosarcoma classification using multilevel feature fusion and ensembles," in *Proc. IEEE 18th India Council Int. Conf. (INDICON)*, India, Dec. 2021, pp. 1–6.

[9] T. Vaiyapuri, A. Jothi, K. Narayanasamy, K. Kamatchi, S. Kadry, and J. Kim, "Design of a honey badger optimization algorithm with a deep transfer learning-based osteosarcoma classification model," *Cancers*, vol. 14, no. 24, p. 6066, Dec. 2022.

[10] F. Gou, J. Liu, J. Zhu, and J. Wu, "A multimodal auxiliary classification system for osteosarcoma histopathological images based on deep active learning," *Healthcare*, vol. 10, no. 11, p. 2189, Oct. 2022.

[11] I. Ahmad, S. Muhammad Israr, and Z. Ul Islam, "A three in one bottom-up framework for simultaneous semantic segmentation, instance segmentation and classification of multi-organ nuclei in digital cancer histology," 2023, *arXiv:2308.11179*.

[12] S. Graham, Q. D. Vu, S. E. A. Raza, A. Azam, Y. W. Tsang, J. T. Kwak, and N. Rajpoot, "Hover-net: Simultaneous segmentation and classification of nuclei in multi-tissue histology images," *Med. Image Anal.*, vol. 58, Jul. 2019, Art. no. 101563.

[13] A. A. Chowdhury, S. H. Mahmud, M. F. Elahe, H. Jahan, W. Shoombuatong, and M. Mahmud, "Detection of osteosarcoma using deep feature extraction with federated learning and MLP from histopathological images," Tech. Rep., 2023, doi: 10.21203/rs.3.rs-3620182/v1.

[14] S. J. Badashah, S. S. Basha, S. R. Ahamed, and S. P. V. Subba Rao, "Fractional-Harris hawks optimization-based generative adversarial network for osteosarcoma detection using Renyi entropy-hybrid fusion," *Int. J. Intell. Syst.*, vol. 36, no. 10, pp. 6007–6031, Oct. 2021.

[15] P. Bansal, K. Gehlot, A. Singhal, and A. Gupta, "Automatic detection of osteosarcoma based on integrated features and feature selection using binary arithmetic optimization algorithm," *Multimedia Tools Appl.*, vol. 81, no. 6, pp. 8807–8834, Mar. 2022.

[16] S. Prabakaran and S. Mary Praveena, "Robust hyperparameter tuned deep Elman neural network for the diagnosis of osteosarcoma on histology images," *J. Intell. Fuzzy Syst.*, vol. 45, no. 4, pp. 5987–6003, Oct. 2023.

[17] I. Ahmed, H. Sardar, H. Aljuaid, F. Alam Khan, M. Nawaz, and A. Awais, "Convolutional neural network for histopathological osteosarcoma image classification," *Comput., Mater. Continua*, vol. 69, no. 3, pp. 3365–3381, 2021.

[18] Y. Shen, F. Gou, and Z. Dai, "Osteosarcoma MRI image-assisted segmentation system base on guided aggregated bilateral network," *Mathematics*, vol. 10, no. 7, p. 1090, Mar. 2022.

[19] L. Asito, H. Pereira, M. Nogueira-Barbosa, and R. Tinós, "Detection of osteosarcoma on bone radiographs using convolutional neural networks," in *Proc. Anais do Congresso Brasileiro de Inteligência Computacional*, Joinville, Brasil, Jan. 2021, pp. 3–6.

[20] M. T. Aziz, S. M. H. Mahmud, M. F. Elahe, H. Jahan, M. H. Rahman, D. Nandi, L. K. Smirani, K. Ahmed, F. M. Bui, and M. A. Moni, "A novel hybrid approach for classifying osteosarcoma using deep feature extraction and multilayer perceptron," *Diagnostics*, vol. 13, no. 12, p. 2106, Jun. 2023.

[21] N. Priyadharshini, B. Hemalatha, and C. Sureshkumar, "A novel hybrid extreme learning machine and teaching–learning-based-optimization algorithm for skin cancer detection," *Healthcare Analytics*, vol. 3, Nov. 2023, Art. no. 100161.

[22] A. B. Eysa and S. Kurnaz, "Diagnose colon disease by feature selection based on artificial neural network and group teaching optimization algorithm," *Optik*, vol. 271, Dec. 2022, Art. no. 170166.

[23] S. Lal, D. Das, K. Alabhya, A. Kanfade, A. Kumar, and J. Kini, "NucleiSegNet: Robust deep learning architecture for the nuclei segmentation of liver cancer histopathology images," *Comput. Biol. Med.*, vol. 128, Jan. 2021, Art. no. 104075.

[24] I. Ahmad, Y. Xia, H. Cui, and Z. U. Islam, "DAN-NucNet: A dual attention based framework for nuclei segmentation in cancer histology images under wild clinical conditions," *Exp. Syst. Appl.*, vol. 213, Mar. 2023, Art. no. 118945.

[25] Z. Rahman, Y.-F. Pu, M. Aamir, and F. Ullah, "A framework for fast automatic image cropping based on deep saliency map detection and Gaussian filter," *Int. J. Comput. Appl.*, vol. 41, no. 3, pp. 207–217, May 2019.

[26] M. K. Naim, T. R. Mengko, R. Hertadi, A. Purwarianti, and M. Susanty, "EmbedCaps-DBP: Predicting DNA-binding proteins using protein sequence embedding and capsule network," *IEEE Access*, vol. 11, pp. 121256–121268, 2023.

[27] X. Chen, F. Xu, and K. He, "Multi-region combined heat and power economic dispatch based on modified group teaching optimization algorithm," *Int. J. Electr. Power Energy Syst.*, vol. 155, Jan. 2024, Art. no. 109586.

[28] J. Zhang, X. Qi, and G. Ji, "Self attention based bi-directional long short-term memory auto encoder for video anomaly detection," in *Proc. 9th Int. Conf. Adv. Cloud Big Data (CBD)*, Mar. 2022, pp. 107–112.